

This discussion paper is/has been under review for the journal Atmospheric Chemistry and Physics (ACP). Please refer to the corresponding final paper in ACP if available.

Chemical composition and sources of coastal marine aerosol particles during the 2008 VOCALS-REx campaign

Y.-N. Lee¹, S. Springston¹, J. Jayne², J. Wang¹, J. Hubbe³, G. Senum¹, L. Kleinman¹, and P. H. Daum¹

¹Atmospheric Sciences Division, Brookhaven National Laboratory, Upton, NY 11973, USA

²Aerodyne Research Inc., Bellerica, MA 01821, USA

³Pacific Northwest National Laboratory, P. O. Box 999, K8-88, Richland, WA 99352, USA

Received: 3 September 2013 – Accepted: 4 September 2013 – Published: 9 October 2013

Correspondence to: P. H. Daum (phdaum@bnl.gov)

Published by Copernicus Publications on behalf of the European Geosciences Union.

26043

Abstract

The chemical composition of aerosol particles ($D_p \leq 1.5 \mu\text{m}$) was measured over the southeast Pacific ocean during the VOCALS-REx experiment between 16 October and 15 November 2008 using the US DOE G-1 aircraft. The objective of these flights was to gain an understanding of the sources and evolution of these aerosols, and how they interacted with the marine stratus cloud layer that prevails in this region of the globe. Our measurements showed that the marine boundary layer (MBL) aerosol mass was dominated by non-sea-salt SO_4^{2-} , followed by Na^+ , Cl^- , Org, NH_4^+ , and NO_3^- , in decreasing order of importance; CH_3SO_3^- (MSA), Ca^{2+} , and K^+ rarely exceeded their limits of detection of ~ 0.05 and $\sim 0.15 \mu\text{g m}^{-3}$ for anions and cations, respectively. The aerosols were strongly acidic as the NH_4^+ to SO_4^{2-} equivalence ratio was typically < 0.3 ; this inferred acidity is corroborated by the conductivity of aqueous samples collected by the PILS. Sea-salt aerosol (SSA) particles, represented by NaCl , showed Cl^- deficits caused by both HNO_3 and H_2SO_4 , and were externally mixed with SO_4^{2-} particles as the AMS detected no NO_3^- whilst uptake of HNO_3 occurred only on SSA particles. The SSA loading as a function of wind speed agreed with that calculated from published relationships, and contributed only a small fraction of the total accumulation mode particle number. Vertical distribution of MBL SSA particles ($D_p \leq \sim 1.5 \mu\text{m}$) was uniform, suggesting a very limited dilution from entrainment of free tropospheric (FT) air. It was inferred that because all of the aerosol species (except SSA) exhibited a strong land-to-sea gradient, they were of continental origin. Comparison of relative changes in median values using LOWESS fits as proxies suggests that (1) an oceanic source of NH_3 is present between 72°W and 76°W , and (2) additional organic aerosols from biomass burns or biogenic precursors were emitted from coastal regions south of 31°S , with possible cloud processing, and (3) FT contributions to MBL gas and aerosols were negligible. Positive Matrix Factorization analysis of organic aerosol mass spectra obtained with the AMS showed an HOA on 28 October 2008 but not on 6 November 2008 that we attribute to a more extensive cloud processing on the later date. A highly ox-

26044

cation of oceanic OA sources in clean MBL air, found that marine contributions to OA in the SEP was nearly absent because even the very low OA loadings in clean marine air ($\text{CO} < 61 \text{ ppb}$) were associated with the combustion tracer black carbon. Allen et al. (2011) showed the strong influence of continental emissions to aerosols in the MBL of the SEP east of 80°W , and long range transport of biomass burn plumes rich in OA to the FT in the SEP region. A SO_4^{2-} concentration of $0.3 \mu\text{g m}^{-3}$ observed in the MBL was considered a background value of the VOCALS region. In this work we report the loadings and chemical composition of fine aerosol particles ($D_p < 1.5 \mu\text{m}$), measured on board the DOE G-1 in the coastal marine atmospheres off northern Chile using both an Aerosol Mass Spectrometer and a Particle-into-liquid Sampler – Ion Chromatography technique, up to $\sim 780 \text{ km}$ off shore (77.8°W) between 18.4°S and 20°S . Complementing earlier reports, we examine the sources and evolution of aerosol particles to provide additional characterization of the relative importance of land, ocean, and FT contributions to aerosols that serve as cloud precursors in the coastal MBL of the SEP.

2 Experimental section

The instrumented DOE G-1 aircraft deployed in the VOCALS was supported by the DOE Atmospheric Sciences Program and was among three other aircraft stationed at Arica International Airport, Chile ($18^\circ 27.44' \text{S}$, $70^\circ 22.37' \text{W}$): NSF C130, UK BAAM Bae-146, and UK NERC Dornier 228 (Wood et al., 2011). The G-1 was equipped with a suite of aerosol and cloud instrumentation for characterizing aerosol chemical composition as well as aerosol and cloud microphysics (Allen, 2011). The study took place over the coastal waters off Northern Chile in the SEP between 15 October and 15 November 2008. The G-1 conducted 17 research flights mainly between 18°S and 20°S , extending west up to $\sim 78^\circ \text{W}$ (Fig. 1), typically between 11 a.m. and 3 p.m. local time (LT), each lasting 3–4 h. The date and time of the flights are listed in Table 1.

26047

2.1 Instrumentation

The G-1 was equipped with instruments for characterizing aerosol particles, cloud droplets, trace gas species, atmospheric state parameters and winds (Kleinman et al., 2012). The instruments for determining aerosol chemical composition and size distributions are briefly described below; CO , O_3 , and SO_2 instruments are described elsewhere (Springston et al., 2005).

2.1.1 Aerosol mass spectrometer

An Aerodyne Compact Time-of-Flight Aerosol Mass Spectrometer (AMS) was deployed to determine the chemical composition of non-refractory particles in the size range $D_p \sim 70 \text{ nm}$ to 440 nm . In order to maintain a constant transmission efficiency of the particle focusing lens on the AMS within the altitude range of the G-1 during VOCALS (up to $\sim 3 \text{ km}$), a constant pressure chamber maintained at 650 mbar was outfitted upstream of the AMS inlet so that the pressure drop across a pinhole into the AMS was independent of flight altitude. The AMS measurement alternated between the mass spectrometer and the particle time-of-flight (pToF) mode of operation, each complete cycle taking $\sim 22 \text{ s}$ which is the time resolution of the AMS data. The pToF measurements determined the vacuum aerodynamic diameter (D_{VA}) of the particles. The chemical species quantified included NH_4^+ , SO_4^{2-} , NO_3^- , Cl^- , and Org (total organics), limits of detection (LOD) being $\sim 0.1 \mu\text{g m}^{-3}$ for NO_3^- , Cl^- , and SO_4^{2-} , and $\sim 0.2 \mu\text{g m}^{-3}$ for NH_4^+ and Org. A description of the AMS instrument is given by Drewnick et al. (2005).

2.1.2 Particle-into-Liquid Sampler – Ion Chromatography (PILS-IC)

A PILS system (Orsini et al., 2003) was used to determine the bulk chemical composition of particles in the size range $D_p \sim 70 \text{ nm}$ – $\sim 1.5 \mu\text{m}$, the upper size cut being limited by the isokinetic inlet outfitted on the G-1 (see below). The species quantified by

26048

3.3.2 28 October 2008 flight

The G-1 flew west along 18.5° S after taking off at 9.58 a.m. LT and repeated a below-, in-, and above-cloud staircase pattern until reaching the westernmost point (77.8° W, Fig. 3a). The BC transects during the outbound segment were at ~ 600 m. After turning around and headed to Arica, the G-1 sampled MBL air at 100 m until making an approach for landing. The BC NH_4^+ , SO_4^{2-} , Org, and NO_3^- concentrations which showed a clear land-to-sea gradient, were nearly invariant at a given location during the 4 h flight period, the values at 600 m (outbound) and at 100 m (inbound) being identical to within 10 % (Fig. 3b and c). In contrast, concentrations of Na^+ and Cl^- , representing SSA particles, were rather constant longitudinally; the Cl^- deficit, caused by uptake of gas phase HNO_3 and in-cloud H_2SO_4 production, was more pronounced near the shore (Fig. 3d). Concentrations of all aerosol species dropped significantly during in-cloud segments (colored sections of the altitude trace in Fig. 3a) because aerosol particles turned cloud droplets were not detected by the AMS and the PILS. The AC air also showed much lower concentrations of most of the species than observed in BC, reflecting a generally cleaner conditions of the FT whose air masses are typically derived from long range transport, thereby more aged and had undergone cloud processing by which soluble substances had been removed (Kleinman et al., 2012).

3.4 Ensemble aerosol chemical composition

The clear air aerosol chemical composition determined for the entire mission is examined in this section to allow composite horizontal and vertical distribution patterns to be characterized. The data are segregated into the BC ($\text{RH} > 50\%$ and $\text{LWC} < 0.01 \text{ g m}^{-3}$) and AC ($\text{RH} < 45\%$ and $\text{LWC} < 0.01 \text{ g m}^{-3}$) regions. We point out that some of the samples identified as AC, in particular those near the shore, had no clouds below them, but are assigned as FT based on potential temperature data. Some AC data were below the inversion, devoid of clouds but remained moist. In this work, AC is interchangeably used with FT.

26053

3.4.1 Composite longitudinal distributions

Concentrations of BC SO_4^{2-} , NH_4^+ , and Org determined using the AMS and Na^+ and NO_3^- determined using the PILS are plotted as a function of longitude in Fig. 4. Overlaid on the data points are box plots of one-degree binned data in longitude for SO_4^{2-} , NH_4^+ , and Org, and two-degree binned data (separated by -72 , -74 , and -76°W) for Na^+ and NO_3^- . AC concentrations of these 5 species are plotted analogously, but with RH shown to identify recent surface contacts (Fig. 5). All the box plots in this work show the median and the inner quartiles by the center, bottom, and top cross bars of the rectangular boxes, and the 5 % and 95 % ranges by the whiskers.

Although box plots are commonly used to summarize data patterns with centers and spreads, they are stepwise because of binning. In order to present data patterns in a continuous fashion to facilitate comparisons, we utilize the Locally Weighted Scatter Smoothing lines, LOWESS (Cleveland, 1979), to supplement the box plot approach. Being insensitive to outliers, LOWESS fits closely approximate median values, and deviate only when data density significantly drops. The suitability of this approach is demonstrated in Figs. 4 and 5 where the LOWESS fits agree well with the median values defined by the boxplots except for the westernmost bins where they diverge slightly.

The LOWESS fits, as proxy for medians, exhibit pronounced land-to-sea gradients in the BC concentrations of SO_4^{2-} , NH_4^+ , Org, and NO_3^- (Fig. 4). In contrast, the median of Na^+ , representing SSA, exhibited a rather uniform longitudinal distribution, increasing slightly offshore. These gradients are consistent with a continental source for SO_4^{2-} , NH_4^+ , Org, and NO_3^- . The median AC concentrations of SO_4^{2-} and NH_4^+ (Fig. 5) also exhibited a land-to-sea gradient, showing the influence of nearby terrestrial sources, likely in Chile and Peru (Allen et al., 2011). Higher AC concentrations of SO_4^{2-} , NH_4^+ , as well as Org, near the shore (east of $\sim 73^\circ \text{W}$) were associated with moist air (RH up to $\sim 50\%$, Fig. 5) that was likely transported vertically from surface by diurnal pumping in the steep coastal terrain followed by advection to the Pacific (Bretherton et al., 2010;

26054

we can attribute the loss of SSA-bound NO_3^- to preferential removal of SSA particles through drizzle because of their larger sizes (Twohey et al., 2012), we note that the SSA loadings in samples where $[\text{NO}_3^-] = 0$ were only a factor of ~ 2 lower than those with $[\text{NO}_3^-] > 0$. This suggests SSA particles, at least those with $D_p \leq 2 \mu\text{m}$, are rapidly replenished after precipitation events.

The observed aerosol NO_3^- concentrations only explained a portion of the Cl^- deficit: with NO_3^- taken into account, a $\sim 25\%$ Cl^- deficit remains, presumably due to H_2SO_4 . Incorporating H_2SO_4 into SSA can in principle be achieved by uptaking of gaseous H_2SO_4 , coagulation with sulfate aerosols, and in-cloud oxidation of SO_2 . The rate of collision coalescence of SSA with sulfate aerosols is too slow to be important for acidifying SSA. The characteristic time constant for removing SO_4^{2-} particles at SSA particle concentration of $\sim 4 \text{cm}^{-3}$ and a coalescence coefficient of $K \leq 5 \times 10^{-9} \text{cm}^3 \text{s}^{-1}$ is estimated to be ≥ 500 days. Although in-cloud aqueous oxidation process can in principle be important considering its fast reaction kinetics and the prevalence of cloud in the study region, a quantitative evaluation is unfortunately untenable because the key oxidant H_2O_2 was not determined and the concentration of SO_2 was always below the LOD of our instrument of 0.2 ppb.

4.5 Composite longitudinal distributions of aerosol and gas constituents

The composite longitudinal distributions of SO_4^{2-} , NH_4^+ , and Org taken as their LOWESS fits normalized to their maximum concentrations at the easternmost location (see, e.g., Fig. 5) are shown in Fig. 19a. These median concentrations decreased steeply with distance from land indicating their continental origins. The longitudinal gradients observed in a narrow latitude band ($\sim 19^\circ \text{S}$) reflects medians of the remaining concentrations of continental emissions advected into the MBL. According to back trajectory calculations by Allen et al. (2011, Fig. 4), continental emissions received along the 20°S parallel from the coast to the open ocean originated from the Chilean coast moving progressively southward. The 5 day back trajectories originating from

26065

20°S show that for 72°W and 76°W , land contact occurred at around 26°S – 30°S and 30°S – 40°S , respectively. However, since the back trajectories also show that because of the wind speed gradient, higher off shore, the ages of the air masses sampled along the 19°S parallel since land contact were roughly comparable (~ 3 – 4 days). Consequently we surmise that the emissions had been aged and processed when sampled, and the longitudinal concentration gradients were due mainly to a higher degree of dilution with higher wind speed off shore. This dilution characteristics is roughly approximated by the normalized longitudinal distribution of the conservative tracer CO (Fig. 19a) provided the CO emission factor remained relatively invariant, and that an appropriate background value can be assigned. Regarding the latter, we chose 62 ppb, the average of the lowest 5% [CO], which is similar to the 61 ppb used by Shank et al. (2012). Since background air can have different levels of CO depending on its history, choosing a single value to estimate the excess CO ($[\text{CO}]_{\text{ex}}$) has a relatively large uncertainty for regions of fairly low total [CO]. Finally, the fact that the highest $[\text{CO}]_{\text{ex}}$ near the shore was only ~ 14 ppb indicates that a significant dilution had occurred to the emissions from the sources considering a typical urban $[\text{CO}]_{\text{ex}}$ of ~ 200 ppb and greater.

Atmospheric concentration of a trace species decreases with dilution and removal, and increases with additional emissions and/or production. In the VOCALS study domain, the factors governing aerosol/trace gas evolution in the MBL may be simplified because of a uniform wind field, somewhat homogenized (by the southerlies along the coast) regional urban and industrial emission characteristics, and the lack of appreciable oceanic sources. Large point sources such as smelters located typically at higher altitudes along the Chilean caldera were found to contribute minimally to MBL aerosol loadings during VOCALS (Twohey et al., 2012). However, in principle, one emission that may manifest a varied longitudinal impact along 19°S parallel is continental biogenic emissions which are potentially important only from south of $\sim 31^\circ \text{S}$, as the arid Atacama desert lying north is devoid of any significant biological activity. Consequently, the near shore segments of the G-1 flights along $\sim 19^\circ \text{S}$ received nearby continental emissions (e.g., urban, industry, and dust) with little biogenic contributions, but the

26066

4.8 Identification of organosulfur compounds

The OOA mass spectra identified for both 28 October 2008 and 6 November 2008 flights, which resembles that for fulvic acid, also contain mass fragments m/z 79 (CH_3SO_2^+) and m/z 96 ($\text{CH}_3\text{SO}_3\text{H}^+$), indicative of MSA (Phinney et al., 2006; Zorn et al., 2008). Since MSA is a product of DMS which serves as the most important precursor of marine SO_4^{2-} aerosol, its characterization is crucial for understanding DMS's contribution to the marine environment. In terms of detection, we keep in mind that any MSA produced in the gas phase is expected to be sequestered in SSA particles (e.g., Hopkins et al., 2008) as refractory sodium salt, exhibiting low CE. Attempting to isolate a MSA factor, we repeated the PMF analyses on 28 October 2008 and 6 November 2008 data using $P = 5$ (Fig. 23) and $P = 6$ (Fig. 24), respectively, that were found necessary to separate the MSA factor, although the highest factor in each analysis was of unknown chemical nature in minute amounts. Comparison of the MSA factor with a MSA mass spectrum obtained on an AMS (Phinney et al., 2006) showed a high degree of correspondence, recognizing that the m/z 48 and m/z 64 signals are missing because they have been removed by the AMS algorithm for SO_4^{2-} quantification. The m/z 81 (SO_3H^+) was the only major fragment missing from both MSA mass spectrum profiles, suggesting the absence of acidic MSA. The MSA mass spectrum factors obtained from the two different flights showed a strong correlation (Fig. 25), even though fragments m/z 12 and m/z 45 appeared only on 28 October 2008 but not on 6 November 2008 perhaps due to a lessened cloud processing of the former. Based on these considerations, we conclude that there is a strong likelihood that the MSA factor represents the MSA species. However, while we are unsure of the CE of MSA which was presumably SSA particle bound, we assert that it was not derived from oceanic DMS. We note the longitudinal distributions of MSA (the time series profile) observed on both 28 October 2008 and 6 November 2008 were strongly correlated with SO_4^{2-} (Fig. 23 and Fig. 24) west of 73° W, suggesting co-emitted or co-located sources of these two species and/or their precursors. Although this correlation appeared to be missing east

26075

of 73° W on both days, a similar trend in MSA and SO_4^{2-} could be discerned albeit with a gradually increasing MSA to SO_4^{2-} ratio with distance from the shore. Although MSA has been extensively investigated as a marine atmospheric constituent from DMS oxidation, its presence in continental air has not been characterized in detail. Hueber et al. (1996) reported a higher level of MSA in polluted air advected from the continent than in air of marine origin, but did not examine continental sources as one of the possible explanations.

Another plausible organosulfur compound that could explain this MSA factor, is hydroxymethanesulfonic acid (HMSA). Produced in the liquid phase (e.g., in-cloud) from S(VI) and formaldehyde, HMSA is found near source regions in aerosol particles (Dixon and Aasen, 1999) as well as in cloud and fog waters (Munger et al., 1984; Rao and Collett Jr., 1995; Dall'Osto et al., 2009). HMSA is stable under acidic conditions and decomposes to HSO_3^- and H_2CO at a rate constant of $4.8 (-7) \text{ s}^{-1}$ and $3.5 (-6) \text{ s}^{-1}$ at $\text{pH} = 4$ and $\text{pH} = 5$, respectively (Kok et al., 1986), corresponding to a characteristic time of ~ 80 h at $\text{pH} = 5$, and longer at lower pH. Although HMSA seems not consistent with the m/z 15 methyl fragment found in the MSA mass spectrum, we cannot completely rule out this candidate until its mass spectrum is firmly established on the AMS. We note that Hawkins et al. (2010) have identified organosulfates during VOCALS that were correlated with acidic aerosol sulfate originating from the continent. Since organosulfate formation involves acid catalysis (Surratt et al., 2008), we expect this product to be present in the non-refractory acidic sulfate particles and therefore detected by the AMS. The identification of organosulfate is based on C-O-S stretching at 876 cm^{-1} representing esters of either sulfate or sulfite (Maria et al., 2003). The MSA factor mass spectrum may be explained by a methyl ester of sulfonic acid as an organosulfate, whose mass spectrum on the AMS should aid the interpretation of the data observed here.

The mass spectrum of factor 1 resembles fulvic acid, oxalic acid (Alfarra, 2004), aerosols from smoldering fir and beech fires (Weimer et al., 2008), as well as that of a factor identified as continental in origin, all being extensively oxidized (Chang et al.,

26076

≥ 50% of the total aerosol mass concentration; total organic aerosol (Org) and NH_4^+ each contributed only < 15%. Aerosol NO_3^- was found to reside on SSA particles, externally mixed with SO_4^{2-} particles, resulting from uptake of gaseous HNO_3 by SSA giving rise to a portion of the observed chloride deficit. Concentrations of MBL aerosol SO_4^{2-} , NH_4^+ , Org, and NO_3^- all exhibited a strong longitudinal gradient decreasing with distance from the shore, consistent with their continental origins. In contrast, SSA loading represented by Na^+ was fairly uniform in the MBL with a slight increase off shore where wind speeds were higher. The observed SSA mass loading agreed with the canonical wind speed dependence reported in the literature; the coastal surf zone SSA production was found to contribute to SSA loading at distances as far as to ~ 400 km offshore. Number concentration of SSA was much smaller than that for SO_4^{2-} aerosols even at ~ 78° W, ~ 800 km from the shore. Accumulation mode SSA loading showed a uniform vertical distribution and can in principle be used as a tracer to assess the extent of dilution of MBL due to entrainment of FT air. MSA, an oxidation product of DMS, was all but absent, indicating a minimal role played by DMS from the ocean in sulfur chemistry within the G-1 study domain. Relative changes in distribution patterns in simultaneously measured aerosol species suggest that sources beyond those from urban and industrial regions exist for NH_3 , likely of oceanic origin, and for OA, likely from continental biogenic sources south of Acatama desert. In contrast, concentrations of MBL aerosol NO_3^- and SO_4^{2-} tracked each other and appeared to be entirely attributable to continental anthropogenic emissions that were co-emitted or co-located. PMF analysis of OA mass spectra obtained using the AMS showed an HOA on 28 October 2008 that was well correlated with CO, which was however absent on 6 November 2008. We attributed this contrast to a greater extent of cloud processing of the air masses observed on 6 November 2008. A highly oxidized OOA factor correlated with SO_4^{2-} was identified for both flights. The ratio of OOA to SO_4^{2-} was lower near the coast and higher away from the shore because of an increased OOA derived from coastal biogenic emissions south of 31° S. Another OOA factor identified as an organosulfur, possibly

26079

MSA, was also strongly correlated with SO_4^{2-} therefore believed to be of anthropogenic origin. Identity of this MSA factor, possibly including hydroxymethanesulfonic acid and methyl sulfonate, need to be investigated to better understand the transport of S(IV)-aldehydes adducts as sources for remote regions and the formation of organosulfur compounds as SOA.

Acknowledgements. The Atmospheric Sciences Program within the DOE Office of Biological and Environmental Research, which has since been merged into the Atmospheric System Research Program, supported this research. The authors gratefully acknowledge the DOE G-1 flight crew led by Chief Pilot Bob Hannigan for their dedication and professionalism that ensured a safe and productive scientific mission.

References

- Allen, G., Coe, H., Clarke, A., Bretherton, C., Wood, R., Abel, S. J., Barrett, P., Brown, P., George, R., Freitag, S., McNaughton, C., Howell, S., Shank, L., Kapustin, V., Brekhovskikh, V., Kleinman, L., Lee, Y.-N., Springston, S., Toniazzi, T., Krejci, R., Fochesatto, J., Shaw, G., Krecl, P., Brooks, B., McMeeking, G., Bower, K. N., Williams, P. I., Crosier, J., Crawford, I., Connolly, P., Allan, J. D., Covert, D., Bandy, A. R., Russell, L. M., Trembath, J., Bart, M., McQuaid, J. B., Wang, J., and Chand, D.: South East Pacific atmospheric composition and variability sampled along 20° S during VOCALS-REx, *Atmos. Chem. Phys.*, 11, 5237–5262, doi:10.5194/acp-11-5237-2011, 2011.
- Alfarra, R.: Insights into Atmospheric Organic Aerosols Using an Aerosol Mass Spectrometer, Ph.D. Thesis, University of Manchester, 2004.
- Benedict, K. B., Lee, T., and Collett Jr., J. L.: Cloud water composition over the Southeastern Pacific Ocean during the VOCALS Regional Experiment, *Atmos. Environ.*, 46, 104–114, 2012.
- Blando, J. D. and Turpin, B. J.: Secondary organic aerosol formation in cloud and fog droplets: a literature evaluation of plausibility, *Atmos. Environ.*, 34, 1623–1632, 2000.
- Brechtel, F.: Description and Assessment of a New Aerosol Inlet System for the DOE G-1 Research Aircraft, Technical Report, Brechtel Manufacturing, Inc., 2002.

26080

- Kawakami, N., Osada, K., Nishita, C., Yabuki, M., Kobayashi, H., Hara, K., and Shiobara, M.: Factors controlling sea salt modification and dry deposition of nonsea-salt components to the ocean, *J. Geophys. Res.*, 113, D14216, doi:10.1029/2007JD009410, 2008.
- 5 Kleinman, L. I., Daum, P. H., Lee, Y.-N., Senum, G. I., Springston, S. R., Wang, J., Berkowitz, C., Hubbe, J., Zaveri, R. A., Brechtel, F. J., Jayne, J., Onasch, T. B., and Worsnop, D.: Aircraft observations of aerosol composition and ageing in New England and Mid-Atlantic states during the summer 2002 NEAQS Field Campaign, *J. Geophys. Res.*, 112, D09310, doi:10.1029/2006JD007786, 2007.
- 10 Kleinman, L. I., Springston, S. R., Daum, P. H., Lee, Y.-N., Nunnermacker, L. J., Senum, G. I., Wang, J., Weinstein-Lloyd, J., Alexander, M. L., Hubbe, J., Ortega, J., Canagaratna, M. R., and Jayne, J.: The time evolution of aerosol composition over the Mexico City plateau, *Atmos. Chem. Phys.*, 8, 1559–1575, doi:10.5194/acp-8-1559-2008, 2008.
- 15 Kleinman, L. I., Daum, P. H., Lee, Y.-N., Lewis, E. R., Sedlacek III, A. J., Senum, G. I., Springston, S. R., Wang, J., Hubbe, J., Jayne, J., Min, Q., Yum, S. S., and Allen, G.: Aerosol concentration and size distribution measured below, in, and above cloud from the DOE G-1 during VOCALS-REx, *Atmos. Chem. Phys.*, 12, 207–223, doi:10.5194/acp-12-207-2012, 2012.
- Kok, G., Gitlin, S. N., and Lazrus, A. L.: Kinetics of the formation and decomposition of hydroxymethanesulfonate, *J. Geophys. Res.*, 91, 2801–2804, 1986.
- 20 Kroll, J. H. and Seinfeld, J. H.: Chemistry of secondary organic aerosol: formation and evolution of low-volatility organics in the atmosphere, *Atmos. Environ.*, 42, 3593–3624, 2008.
- Lewis, E. R. and Schwartz, S. E.: *Sea Salt Aerosol Production: Mechanisms, Methods, Measurements and Models*, Geophysical Monograph Series, vol. 152, American Geophysical Union, Washington, DC, 413 pp., 2004.
- 25 Lin, P., Yu, J. Z., Engling, G., and Kalberer, M.: Organosulfates in humic-like substance fraction isolated from aerosols at seven locations in East Asia: a study by ultra-high-resolution mass spectrometry, *Environ. Sci. Technol.*, 46, 13118–13127, 2012.
- 30 Maria, S. F., Russell, L. M., Turpin, B. J., Porcja, R. J., Campos, T. L., Weber, R. J., and Huebert, B. J.: Source signatures of carbon monoxide and organic functional groups in Asian Pacific Regional Aerosol Characterization Experiment (ACE-Asia) submicron aerosol types, *J. Geophys. Res. Atmos.*, 108, 8637, doi:10.1029/2003JD003703, 2003.

26083

- Mathew, B. M., Middlebrook, A. M., and Onasch, T. B.: Collection efficiencies in an Aerodyne aerosol mass spectrometer as a function of particle phase for laboratory generated aerosols, *Aerosol Sci. Tech.*, 42, 884–898, 2008.
- 5 Munger, J. W., Jacob, D. J., and Hoffmann, M. R.: The occurrence of bisulfite-aldehyde addition products in fog-and cloudwater, *J. Atmos. Chem.*, 1, 335–350, 1984.
- Ng, N. L., Canagaratna, M. R., Zhang, Q., Jimenez, J. L., Tian, J., Ulbrich, I. M., Kroll, J. H., Docherty, K. S., Chhabra, P. S., Bahreini, R., Murphy, S. M., Seinfeld, J. H., Hildebrandt, L., Donahue, N. M., DeCarlo, P. F., Lanz, V. A., Prévôt, A. S. H., Dinar, E., Rudich, Y., and Worsnop, D. R.: Organic aerosol components observed in Northern Hemispheric datasets from Aerosol Mass Spectrometry, *Atmos. Chem. Phys.*, 10, 4625–4641, doi:10.5194/acp-10-4625-2010, 2010.
- 10 O'Dowd, C. D., Facchini, M. C., Cavalli, F., Ceburnis, D., Mircea, M., Decesari, S., Fuzzi, S., Yoon, Y. J., and Putaud, J.-P.: Biogenically driven organic contribution to marine aerosol, *Nature*, 431, 676–680, 2004.
- 15 Olsen, T. M. and Hoffmann, M. R.: Hydroxyalkylsulfonate formation: its role as a S(IV) reservoir in atmospheric water droplets, *Atmos. Environ.*, 23, 985–997, 1989.
- Orsini, D. A., Ma, Y., Sullivan, A., Sierau, B., Baumann, K., and Weber, R. J.: Refinements to the particle-into-liquid sampler (PILS) for ground and airborne measurements of water soluble aerosol composition, *Atmos. Environ.*, 37, 1243–1259, 2003.
- 20 Parrish, D. D.: Critical evaluation of US on-road vehicle emission inventories, *Atmos. Environ.*, 40, 2288–2300, 2006.
- Phinney, L., Richard Leaitch, W., Lohmann, U., Boudries, H., Worsnop, D. R., Jayne, J. T., Toom-Saunty, D., Wadleigh, M., Sharma, S., and Shantz, N.: Characterization of the aerosol over the sub-arctic North East Pacific Ocean, *Deep-Sea Res. Pt. II*, 53, 2410–2433, doi:10.1016/j.dsr2.2006.05.044, 2006.
- 25 Rahn, D. A. and Garreaud, R.: Marine boundary layer over the subtropical southeast Pacific during VOCALS-REx – Part 1: Mean structure and diurnal cycle, *Atmos. Chem. Phys.*, 10, 4491–4506, doi:10.5194/acp-10-4491-2010, 2010.
- Rao, X. and Collett Jr., J.: Behavior of S(IV) and formaldehyde in a chemically heterogeneous cloud, *Environ. Sci. Technol.*, 29, 1023–1031, 1995.
- 30 Schneider, J., Weimer, S., Drewnick, F., Borrmann, S., Helas, G., Gwaze, P., Schmid, O., Andreae, M. O., and Kirchner, U.: Mass spectrometric analysis and aerodynamic properties of

26084

- various types of combustion-related aerosol particles, *Int. J. Mass Spectrom.*, 258, 37–49, 2006.
- Saide, P. E., Spak, S. N., Carmichael, G. R., Mena-Carrasco, M. A., Yang, Q., Howell, S., Leon, D. C., Snider, J. R., Bandy, A. R., Collett, J. L., Benedict, K. B., de Szoek, S. P., Hawkins, L. N., Allen, G., Crawford, I., Crosier, J., and Springston, S. R.: Evaluating WRF-Chem aerosol indirect effects in Southeast Pacific marine stratocumulus during VOCALS-REx, *Atmos. Chem. Phys.*, 12, 3045–3064, doi:10.5194/acp-12-3045-2012, 2012.
- Schwartz, S. E.: Gas-aqueous reactions of sulfur and nitrogen oxides in liquid-water clouds, in: *SO₂, NO and NO₂ Oxidation Mechanisms: Atmospheric Considerations*, edited by: Calvert, J. G., *Acid Precipitation Series*, vol. 3, Butterworth, Boston, 173–208, 1984.
- Shank, L. M., Howell, S., Clarke, A. D., Freitag, S., Brekhovskikh, V., Kapustin, V., McNaughton, C., Campos, T., and Wood, R.: Organic matter and non-refractory aerosol over the remote Southeast Pacific: oceanic and combustion sources, *Atmos. Chem. Phys.*, 12, 557–576, doi:10.5194/acp-12-557-2012, 2012.
- Slinn, W. G. N.: Air to sea transfer of particles, in: *Air–Sea Exchange of Gases and Particles*, edited by: Liss, P. S. and Slinn, W. G. N., D. Reidel Publishing Co., Dordrecht, Holland, 1983.
- Springston, S. R., Kleinman, L. I., Nunnermacker, L. J., Brechtel, F., Lee, Y.-N., and Wang, J.: Chemical evolution of an isolated power plant plume during the TexAQs 2000 study, *Atmos. Environ.*, 39, 3431–3443, 2005.
- Surratt, J. D., Gómez-González, Y., Chan, A. W. H., Vermeylen, R., Shahgholi, M., Kleindienst, T. E., Edney, E. O., Offenberg, J. H., Lewandowski, M., Jaoui, M., Maenhaut, W., Claeys, M., Flagan, R. C., and Seinfeld, J. H.: Organosulfate formation in biogenic secondary organic aerosol, *J. Phys. Chem. A*, 112, 8345–8378, doi:10.1021/jp802310p, 2008.
- Tang, I. N., Munkelwitz, H. R., and Davis, J. G.: Aerosol growth studies – II. Preparation and growth measurements of monodisperse salt aerosols, *J. Aerosol Sci.*, 8, 149–159, 1977.
- Timko, M. T., Yu, Z., Kroll, J., Jayne, J. T., Worsnop, D. R., Miake-Lye, R. C., Onasch, T. B., Liscinsky, D., Kirchstetter, T. W., Destailats, H., Holder, A. L., Smith, J. D., and Wilson, K. R.: Sampling artifacts from conductive silicone tubing, *Aerosol Sci. Tech.*, 43, 855–865, doi:10.1080/02786820902984811, 2009.
- Tomlinson, J. M., Li, R., and Collins, D. R.: Physical and chemical properties of the aerosol within the southeastern Pacific marine boundary layer, *J. Geophys. Res.*, 112, D12211, doi:10.1029/2006JD007771, 2007.

26085

- Tsapakis, M., Lagoudaki, E., Stephanou, E. G., Kavouras, I. G., Koutrakis, P., Oyola, P., and von Baer, D.: The composition and sources of PM_{2.5} organic aerosol in two urban areas of Chile, *Atmos. Environ.*, 36, 3851–3863, doi:10.1016/S1352-2310(02)00269-8, 2002.
- Twohy, C. H., Anderson, J. R., Toohey, D. W., Andrejczuk, M., Adams, A., Lytle, M., George, R. C., Wood, R., Saide, P., Spak, S., Zuidema, P., and Leon, D.: Impacts of aerosol particles on the microphysical and radiative properties of stratocumulus clouds over the southeast Pacific Ocean, *Atmos. Chem. Phys.*, 13, 2541–2562, doi:10.5194/acp-13-2541-2013, 2013.
- Ulbrich, I. M., Canagaratna, M. R., Zhang, Q., Worsnop, D. R., and Jimenez, J. L.: Interpretation of organic components from Positive Matrix Factorization of aerosol mass spectrometric data, *Atmos. Chem. Phys.*, 9, 2891–2918, doi:10.5194/acp-9-2891-2009, 2009.
- Wang, J., Flagan, R. C., and Seinfeld, J. H.: A Differential Mobility Analyzer (DMA) system for submicron aerosol measurements at ambient relative humidity, *Aerosol Sci. Tech.*, 37, 46–52, doi:10.1080/02786820300891, 2003.
- Weimer, S., Alfarra, M. R., Schreiber, D., Mohr, M., Prévôt, A. S. H., and Baltensperger, U.: Organic aerosol mass spectral signatures from wood-burning emissions: influence of burning conditions and wood type, *J. Geophys. Res. Atmos.*, 113, D10304, doi:10.1029/2007JD009309, 2008.
- Wood, R., Mechoso, C. R., Bretherton, C. S., Weller, R. A., Huebert, B., Straneo, F., Albrecht, B. A., Coe, H., Allen, G., Vaughan, G., Daum, P., Fairall, C., Chand, D., Gallardo Klenner, L., Garreaud, R., Grados, C., Covert, D. S., Bates, T. S., Krejci, R., Russell, L. M., de Szoek, S., Brewer, A., Yuter, S. E., Springston, S. R., Chaigneau, A., Toniazzo, T., Minnis, P., Palikonda, R., Abel, S. J., Brown, W. O. J., Williams, S., Fochesatto, J., Brioude, J., and Bower, K. N.: The VAMOS Ocean-Cloud-Atmosphere-Land Study Regional Experiment (VOCALS-REx): goals, platforms, and field operations, *Atmos. Chem. Phys.*, 11, 627–654, doi:10.5194/acp-11-627-2011, 2011.
- Yang, M., Huebert, B. J., Blomquist, B. W., Howell, S. G., Shank, L. M., McNaughton, C. S., Clarke, A. D., Hawkins, L. N., Russell, L. M., Covert, D. S., Coffman, D. J., Bates, T. S., Quinn, P. K., Zagorac, N., Bandy, A. R., de Szoek, S. P., Zuidema, P. D., Tucker, S. C., Brewer, W. A., Benedict, K. B., and Collett, J. L.: Atmospheric sulfur cycling in the southeastern Pacific – longitudinal distribution, vertical profile, and diel variability observed during VOCALS-REx, *Atmos. Chem. Phys.*, 11, 5079–5097, doi:10.5194/acp-11-5079-2011, 2011.

26086

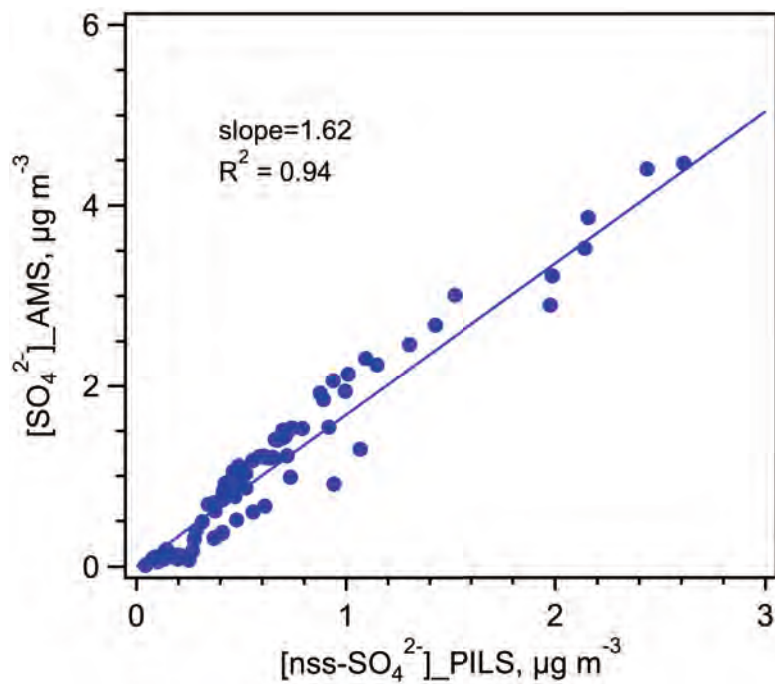


Fig. 2. Correlation of nss-SO₄²⁻ concentrations determined by the AMS and the PILS on 28 October 2008.

26091

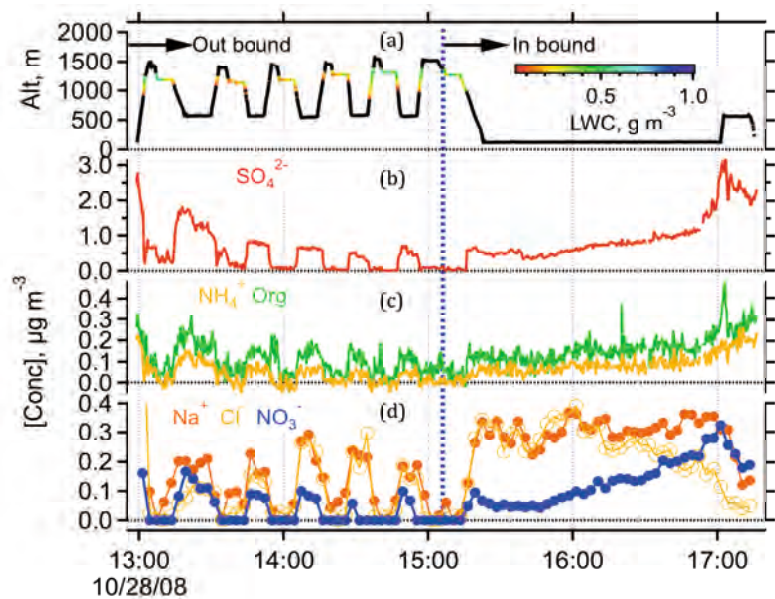


Fig. 3. Time plots of altitude and aerosol chemical concentrations measured on the 28 October 2008 flight. The aircraft altitude plot is color-coded to the liquid water content of clouds encountered during the out-bound leg (panel a); the blue dotted vertical line marks the time when the G-1 turned around and headed back to Arica.

26092

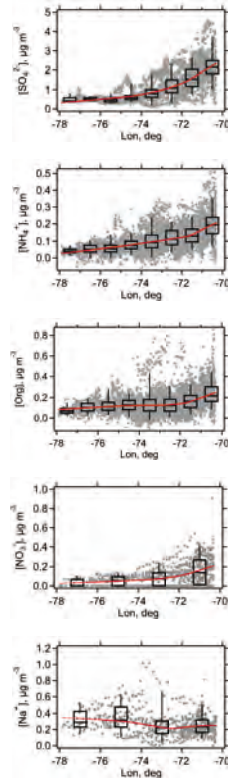


Fig. 4. Composite longitudinal dependence of below cloud (BC) aerosol concentrations determined on the G-1 for the entire VOCALS mission. Box plots (black) and LOWESS fits (red) are overlaid on individual data points (grey).

26093

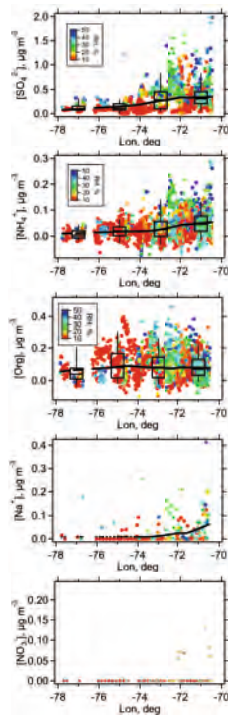


Fig. 5. Composite longitudinal distributions of aerosol concentrations of above cloud (AC) SO_4^{2-} , NH_4^+ , Org, Na^+ , and NO_3^- measured on the G-1 for the entire mission. Data are color coded to RH; solid black line represents LOWESS smooth. Box plots are for two-degree binned data.

26094

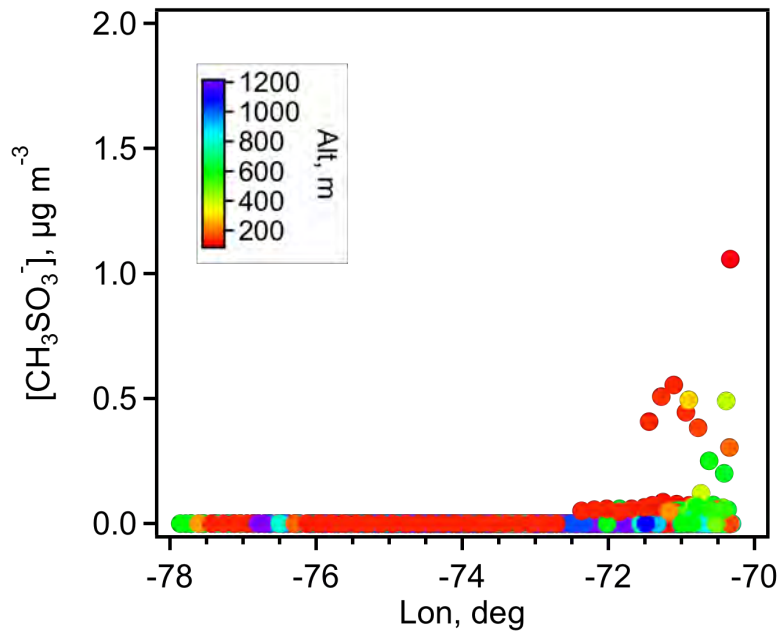


Fig. 6. Longitudinal dependence of aerosol MSA determined using the PILS-IC technique.

26095

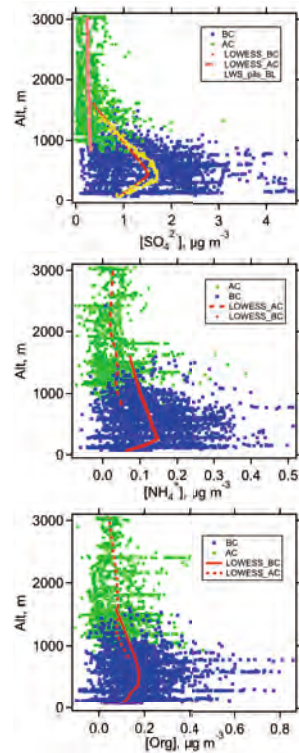


Fig. 7. Composite vertical distributions of the concentrations of SO_4^{2-} , NH_4^+ , and Org for the entire G-1 mission. Continuous lines (dash as well as solid) represent LOWESS fits.

26096

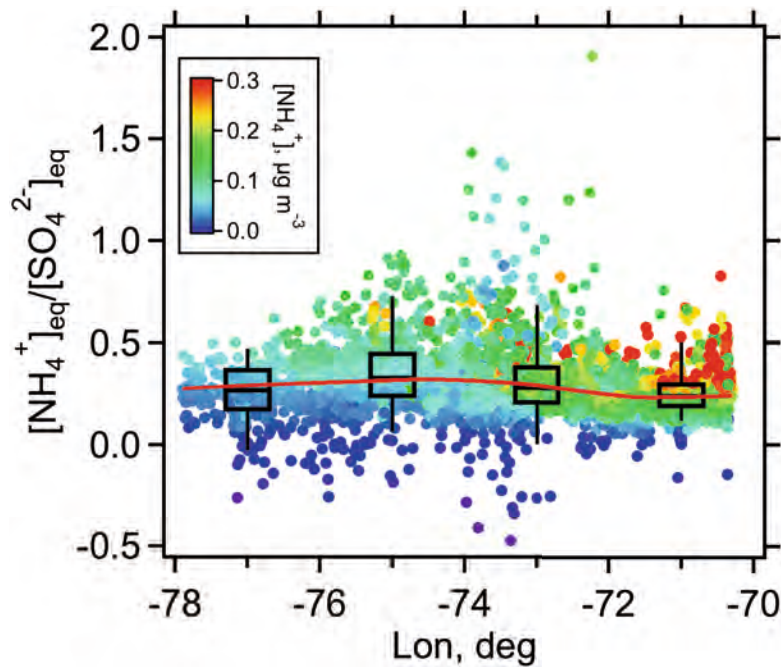


Fig. 10. Longitudinal dependence of the below cloud (BC) aerosol NH_4^+ to SO_4^{2-} equivalence concentration ratio. The red solid trace represents the LOWESS fit, and the box plots summarize the data in four longitude bins, i.e., -70° to -72° , -72° to -74° , -74° to -76° , and -76° to -78° .

26099

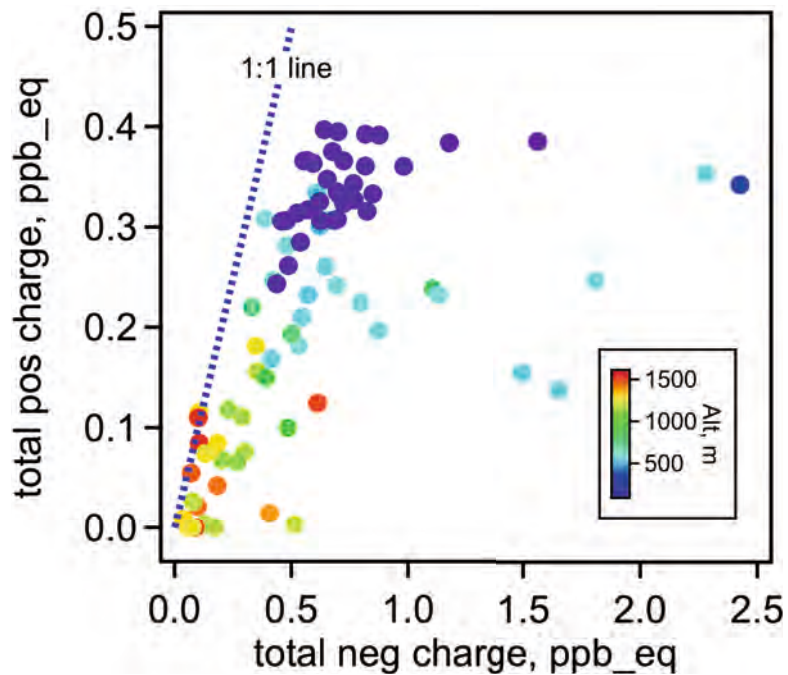


Fig. 11. Charge balance of aerosol components determined using the PILS-IC on 28 October 2008. The units are in parts-per-billion (ppb) multiplied by charge equivalence. Positive ions were dominated by Na^+ and NH_4^+ ; negative by Cl^- , NO_3^- , and SO_4^{2-} .

26100

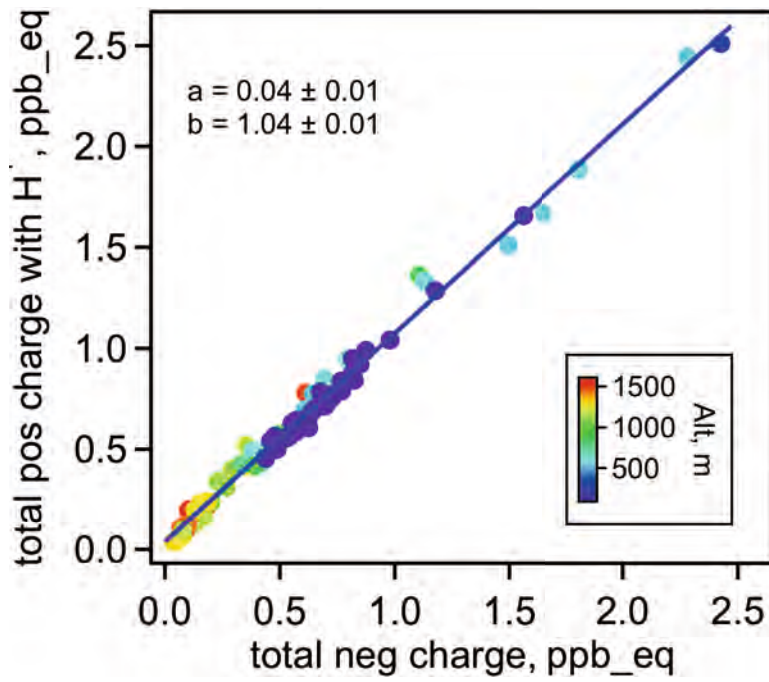


Fig. 12. Same as Fig. 11 except that the total positive charges now include H^+ as the missing cation associated with $nss-SO_4^{2-}$. The straight line represents the least square fit of the data with the values of the intercept, **(a)**, and slope, **(b)**.

26101

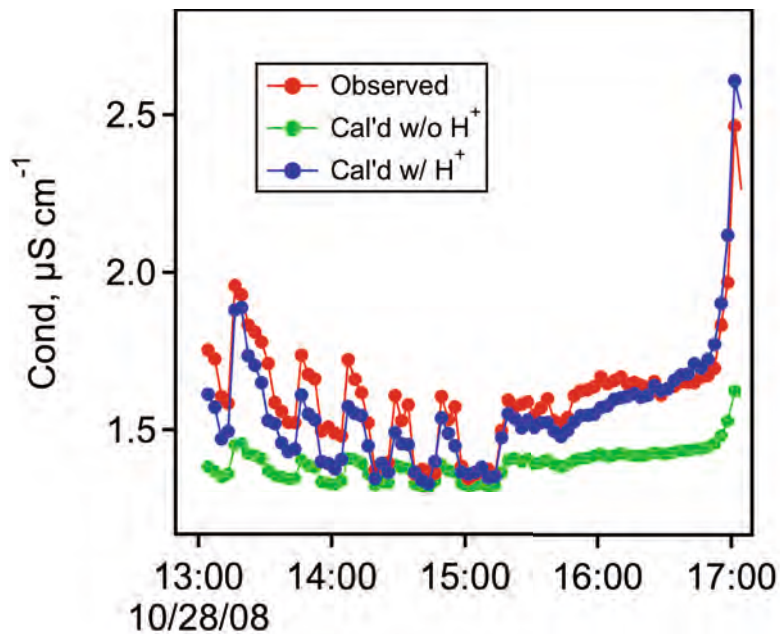


Fig. 13. Comparison of the observed and calculated conductivities of the liquefied aerosol samples collected by the PILS on the 28 October 2008 flight.

26102

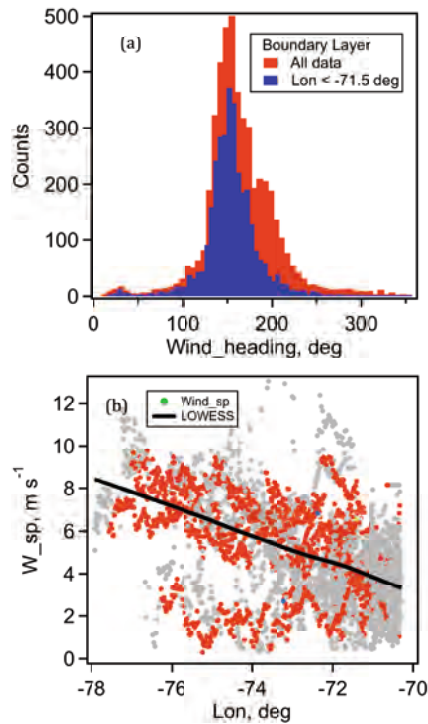


Fig. 14. (a) Histogram of MBL wind directions measured on the G-1 during VOCALS showing a consistent southerly near the coast that shifted slightly towards the NNW (155°) off shore. (b) Wind speed dependence on longitude where the black line represents the LOWESS fits, and the data points in red correspond to altitude less than 150 m.

26103

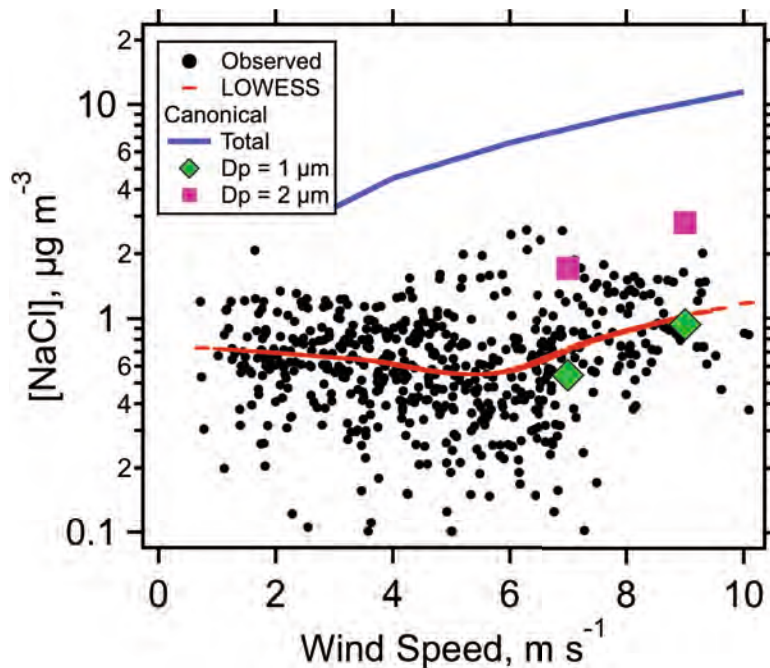


Fig. 15. Wind speed dependence of MBL SSA mass concentration (as NaCl) determined on the G-1 during VOCALS. The solid red line represents the LOWESS fit of the observed NaCl concentrations. The solid blue line represents empirical relationship between the total dry mass of SSA (scaled to NaCl) and the wind velocity at 10 m above sea surface (Fig. 17 in Lewis and Schwartz, 2004). The two sets of symbols in green and magenta represent the calculated concentrations with a $1\ \mu\text{m}$ and $2\ \mu\text{m}$ upper size cut, respectively.

26104

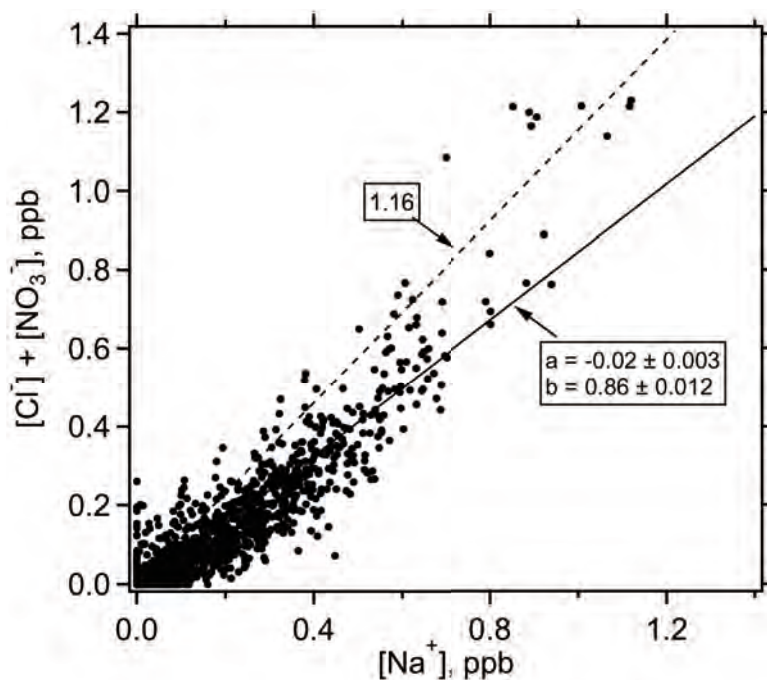


Fig. 18. Relationship between concentrations of aerosol Cl^- and Na^+ with NO_3^- included to account for the displaced Cl^- due to SSA acidification by H_2SO_4 . The dash line represents the sea-water Cl^- to Na^+ ratio of 1.16, and the solid line a least square fit of the data whose intercept and slope are indicated.

26107

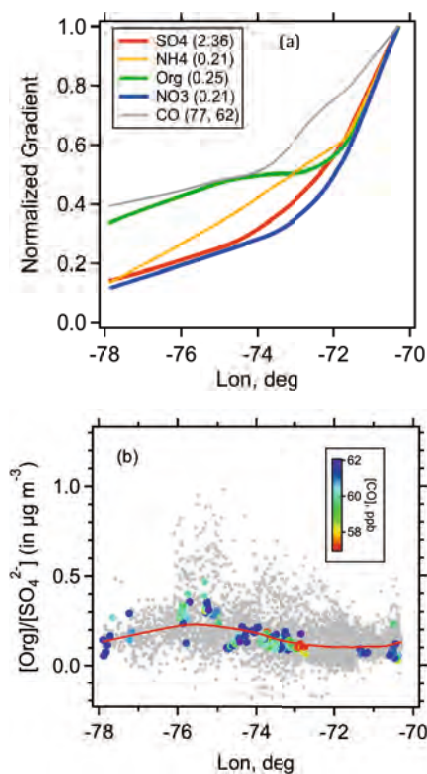


Fig. 19. (a) Normalized composite longitudinal distributions of below-cloud SO_4^{2-} , NH_4^+ , Org, NO_3^- , and CO. **(b)** Dependence of $[\text{Org}]/[\text{SO}_4^{2-}]$ ratio on longitude, where the solid red line represents the LOWESS fit of the data.

26108

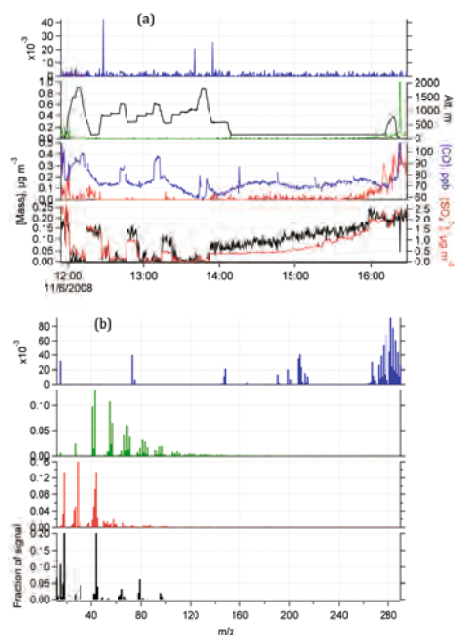


Fig. 22. PMF analysis results of 6 November 2008 data with $p = 4$ and $F_{\text{peak}} = 0.4$. **(a)** Time series of factors 1, 2, 3, and 4 representing mass concentrations shown in black, red, and green, respectively. Overlaid on time series of factors 1, 2, and 3 are $[\text{SO}_4^{2-}]$, $[\text{CO}]$, and flight altitude, respectively. **(b)** Mass spectrum profiles of the 4 factors with the same color designations.

26111

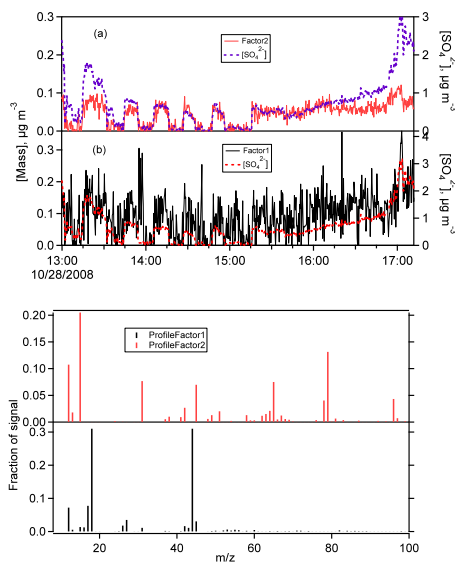


Fig. 23. PMF analysis results of 28 October 2008 data with $p = 5$ and $F_{\text{peak}} = 0$: with only factors 1 and 2 displayed.

26112

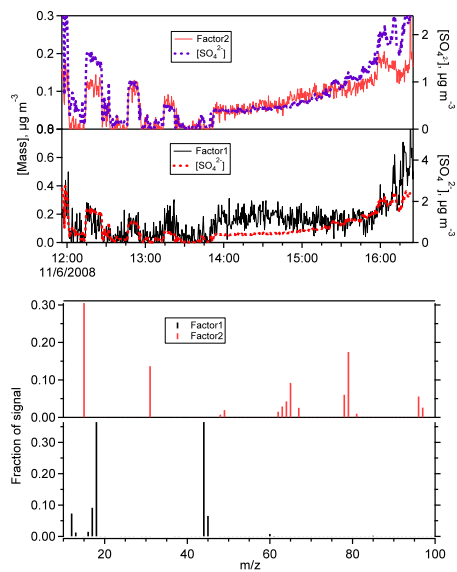


Fig. 24. PMF analysis results of 6 November 2008 data with $p = 6$ and $F_{\text{peak}} = 0.6$: with only factors 1 and 2 displayed.

26113

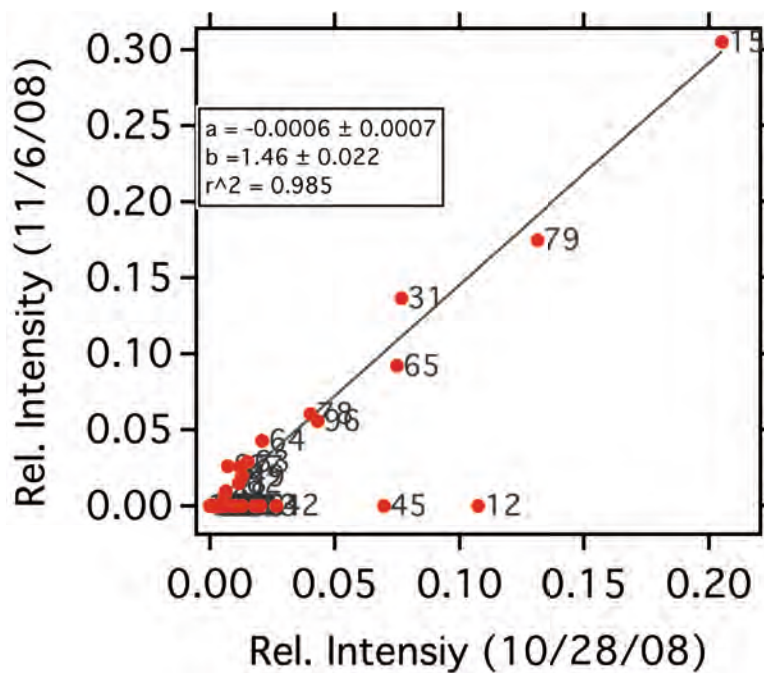


Fig. 25. Correlation of MSA mass spectrum fragments obtained on the 28 October 2008 and 6 November 2008 flights.

26114

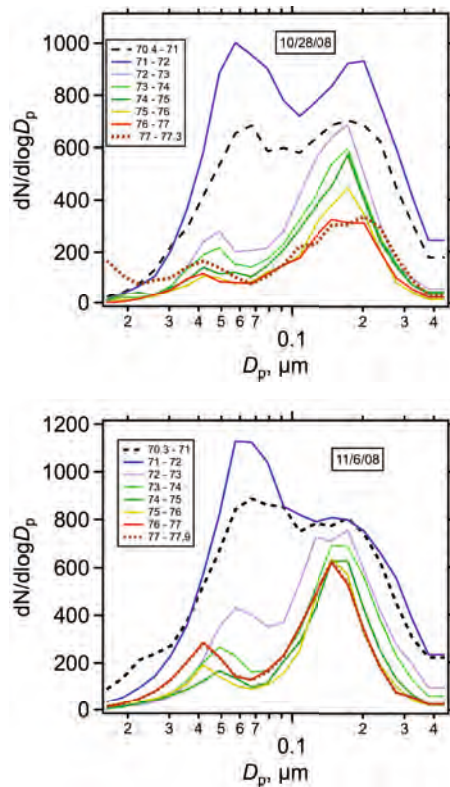


Fig. 26. MBL aerosol particle size distributions during return legs on 28 October 2008 and 6 November 2008 as a function of longitude with data binned into 1-degree intervals.